Egypt. J. Chem. **Vol. 66**, No. 5 pp. 315 - 329 (2023)

Egyptian Journal of Chemistry

http://ejchem.journals.ekb.eg/

Pyrimidine hydrazide ligand and its metal complexes: synthesis, characterization, and antimicrobial activities

S. El-Sayed Saeed [*1], Budoor A. Alomari [1], Ahmed N. Al-Hakimi [1,2], M. M. Abd El-Hady [1,3], Jawza Sh Alnawmasi[1], Hussein H. Elganzory[1], and Wael A. El-Sayed[1,4]

[1] *Department of Chemistry, College of Science, Qassim University, Saudi Arabia.*
[2] *Department of Chemistry, College of Science, Ibb University, Ibb, Yemen*
[3] *National Research Centre (Scopus affiliation ID: 60014618), Institute of Textile Research and Technology, Dokki, Giza 12622, Egypt.*
[4] *Photochemistry Department, National Research Centre, Dokki, Giza 12622, Egypt*.

Abstract

Increasing the resistance to current antimicrobial agents has posed a pressing need for the development of new antimicrobial agents. We, therefore, benefit from the antimicrobial characteristics of pyrimidine derivatives to prepare a new 4-(4-bromophenyl)-6-methyl-2-thioxo-1,2,3,4-tetrahydropyrimidine-5-carbohydrazide ligand. The ligand complexes of (3d; Cr, Mn, Fe, Co, Ni, Cu, and Zn) and 4d -Cd metals are also prepared and characterized by different techniques. The ligand acts as a neutral bidentate and exhibited octahedral geometry. *In vitro*, the antibacterial activity of the ligand and its complexes against *Staphylococcus aureus and Escherichia coli* was investigated. Also, the antifungal against *Candida albicans* and *Aspergillus flavus* was evaluated. The results showed that the produced complexes have antibacterial activity higher than the ligand. The Cd(II) complex showed antifungal activity higher than the other complexes.

Keywords: pyrimidine; hydrazide; metal complexes; antimicrobial

1. Introduction

Hydrazide compounds are widespread in many fields due to their different application. The biological activities of the hydrazide are due to its structure R-CO-NH-NH2 hydrazide. The hydrazide complexes have a promising material in the previous literature because of their bonding to transition metals via various donor atoms (C=O, NH_2, and NH) (1).

Heterocyclic compounds have a wide range of effects on medicinal chemistry due to their huge biological activities. Their varied pharmacological profile, sulfur, nitrogen, and oxygen-containing heterocyclic compounds still attract chemists' and researchers' attention in several areas e.g. antimicrobial (2-4), anticancer (5-7), inks (8, 9), azo disperse dyes (10), antimicrobial (3), Antiproliferative (11).

Pyrimidine heterocyclic core has great value in medicinal chemistry since it comprises the base for thiamine, uracil, and cytosine nitrogen bases which are the building blocks of the nucleic acids (12, 13). Furthermore, pyrimidine derivatives have registered their importance in the development of various pharmaceuticals of broad spectra of therapeutical activities such as anti-microbial (14), anti-viral, anti-HIV (15, 16) anti-tubercular (17, 18) anti-malarial (19-21). The derivatives of 1,2,3,4-tetrahydropyrimidine-2-thiones have been reported to be calcium channel blockers (22), antitumors (23), antidepressant (24), antibacterial (25), and antifungal (26, 27).

Alkhamis, K. et al. prepared N′-cyclohexylidene-3 hydroxy-2-naphthohydrazide ligand. The Cu(II)-hydrazide complex of this ligand displayed a significant binding with DNA and showed anticancer

*Corresponding author e-mail: s.saeed@qu.edu.sa; (S. El-Sayed Saeed).
Receive Date: 06 November 2022, Revise Date: 18 December 2022, Accept Date: 25 December 2022.
DOI: 10.21608/EJCHEM.2022.173181.7161.

activity, while Ni(II) complex showed excellent antioxidants (28). Shakdofa, M. M. et al. prepared 3-(2-(2,4,6-trichlorophenyl) hydrazono) butan-2-one oxime, the copmlexes of this ligand exhibited excellent antimicrobial activities (29). Sawant R. L. et al. prepared 4-(2-Chloro-phenyl)-6-methyl-2-thioxo-1,2,3,4-tetrahydropyrimidine-5-carboxylicacid-N'-[4-(2,4-dioxo-thiazolidin-5-ylidenemethyl)-phenyl]hydrazide, this compound showed antidiabetic activity (30). Younis A. and Awad G. prepared 4-amino-N'-(1-(2-(4-chlorophenyl)hydrazono)-1-(piperidin-1-yl)propan-2-ylidene) benzohydrazide, this hydrazide had excellent antimicrobial activity (31). Gawrońska-Grzywacz, Monika, et al evaluated the antitumor activities of N-[(3-chloro-4-methoxyphenyl)methylidene]-4-methylbenzenesulphonohydrazide, the result showed promising for the against tumours and other diseases related to pathological angiogenesis, such as age-related macular degeneration and diabetic retinopathy (32).

Our aim based on the foregoing the preparation of a ligand "4-(4-Bromophenyl)-6-methyl-2-thioxo-1,2,3,4-tetrahydropyrimidine-5-carbohydrazide and its Cr(III), Mn(II), Fe(III), Co(II), Ni(II), Cu(II), Zn(II) and Cd(II) metal complexes were studied. Also, studying the prepared ligand and its complexes in the as antimicrobial agent.

2. Experimental

2.1 Chemicals

All solvents were obtained from Fisher Scientific. 4-bromobenzaldehyde, ethyl acetoacetate, and thiourea were purchased from Sigma Aldrich. Hydrochloric acid, metal salts, and hydrazine hydrate were purchased from Loba Chemie.

2.2 Instruments:

The UV-Vis spectra were measured by using A Shimadzu (UV-1650PC, Japan) UV-Vis spectrophotometer in DMF solutions (1×10^{-3} M) of the samples. The FTIR spectra of the prepared compounds were measured using an Agilent (Cary 600 FTIR, USA) spectrometer. ^{1}H and ^{13}C NMR (nuclear magnetic resonance) spectroscopies were performed using a Bruker spectrometer (Ascend 400 MHz, USA) at 850 MHz by using DMSO as a solvent; the standard reference was TMS. The CHNS contents of the compounds were measured via a Vario (ELM, Germany). A Shimadzu simultaneous (DTG-60AH, Japan) apparatus was used in with a heating rate of 10 °C per min. The magnetic susceptibility of the complexes at room temp. was measured by magnetic susceptibility balance – auto (Sherwood Scientific, United Kingdom). The JEOL -JEM-1230 transmission electron microscopy (TEM), 40–120 kV accelerating voltage, Japan) was used to measure the size and the shape of the prepared compounds. The x-ray diffraction (XRD) was measured by using A Rigaku (Ultima IV, USA) XRD diffractometer, using Cu Kα radiation (wavelength= 1.54180 Å). The molar conductivity of the samples (1×10^{-3} M) dissolved in DMSO was measured using an Oakton (CON 700, Singapore) conductivity meter.

2.3 Preparation of the ligand

The ligand and the derived prepared metal complexes have been revealed as stable, non-hygroscopic, water-insoluble, partially soluble in ethanol, and freely soluble in DMF and DMSO.

The reaction of the complex formation using ethyl 4-(4-bromophenyl)-6-methyl-2-thioxo-1,2,3,4-tetrahydropyrimidine-5-carboxylate (1) as a ligand (L) with $NiCl_2.6H_2O$, $MnCl_2.4H_2O$, $CuCl_2.2H_2O$, $CoCl_2.6H_2O$, $CrCl_3.6H_2O$, $FeCl_3$(anhydrous), $ZnCl_2$ dry, and $CdCl_2.2.5H_2O$. All the complexes showed to afford with (1M:1L) stoichiometry according to the molar ratio method, but Ni(II) complex showed (1M:2L). The chemical structures, and physical properties of the ligand and its complexes are represented in (Table 1). The observed spectral data as well as the thermal results indicated were in full agreement with the proposed structures.

The ligand was prepared in two steps;

The 1st step is preparation of Ethyl 4-(4-bromophenyl)-6-methyl-2-thioxo-1,2,3,4-tetrahydropyrimidine-5-carboxylate (1)

As shown in (figure 1) and (Scheme 1) a solution of 4-bromobenzaldehyde (2 mmol), ethyl acetoacetate (2.5 mmol), and thiourea (2 mmol) in ethanol (30 mL) and hydrochloric acid (36%, 3-4 drops) was mixed, the reaction mixture refluxed for 6 hrs. The solvent was largely removed to one-third of its original amount and then left to stand at room temperature for 2 hrs. The formed precipitate was filtered, dried in a glass desiccator, and crystallized from EtOH to give the ester 1.

The 2nd step is the preparation of the ligand "4-(4-Bromophenyl)-6-methyl-2-thioxo-1,2,3,4-tetrahydropyrimidine-5-carbohydrazide"

To a solution of the substituted pyrimidine ester 1 (5 mmol) in absolute ethanol (25 mL), was added hydrazine hydrate 99% (6 mmol) and the reactants were heated under reflux for 4 hrs. The solvent was largely removed under reduced pressure and left to stand at room temperature for 3 hours. The afforded precipitate was filtered, dried in a glass desiccator, and crystallized from EtOH to give the hydrazide compound L as yellow crystals.

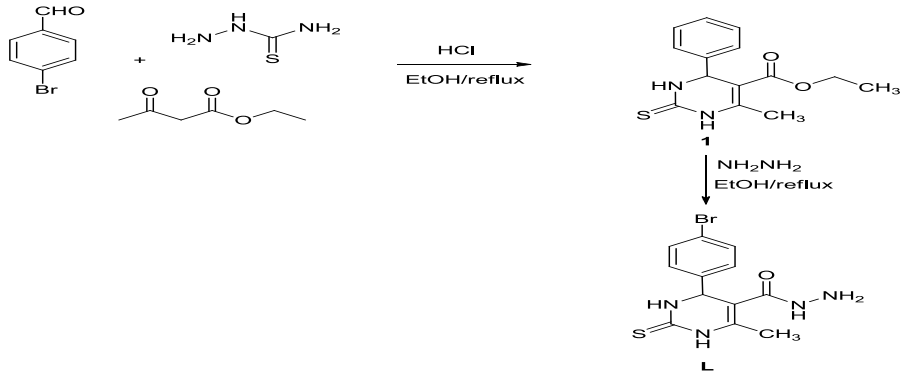

Scheme 1: Synthesis of the Ligand **(L)**.

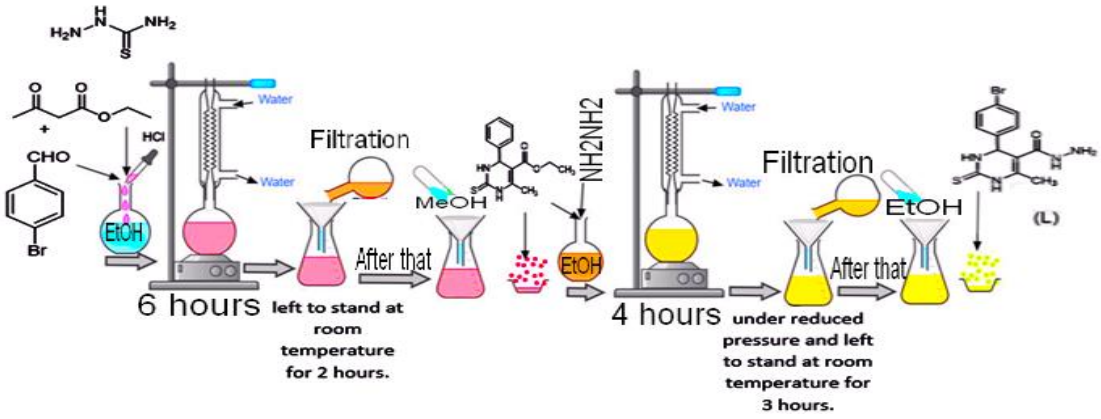

Figure 1: Graphical Scheme of the ligand preparation procedures

2.4 Preparation of the hydrazide metal complexes

The ligand **(L)** metal complexes were prepared by the reactions of **L** with the respective salt by applying this method; As shown in (Scheme 2) a stoichiometric quantity (10 mmol) of ethanolic metal salt solution was mixed with a hot 10 mmol ethanolic solution of the hydrazide ligand except for Ni complex the used **L** was 20 mmol, and then were stirred under reflux. The precipitate was formed in all metals after 5 hours except Ni(II) gave precipitate after 9 hours after adding drops of triethylamine. The resultant solutions were then evaporated to one-third of their original volume. The afforded metal complexes were filtered off, washed with ethanol, and dried in a glass desiccator over anhydrous $CaCl_2$ to give the trivalent (Cr, Fe) and divalent (Mn, Co, Ni, Cu, Zn, and Cd) metal complexes.

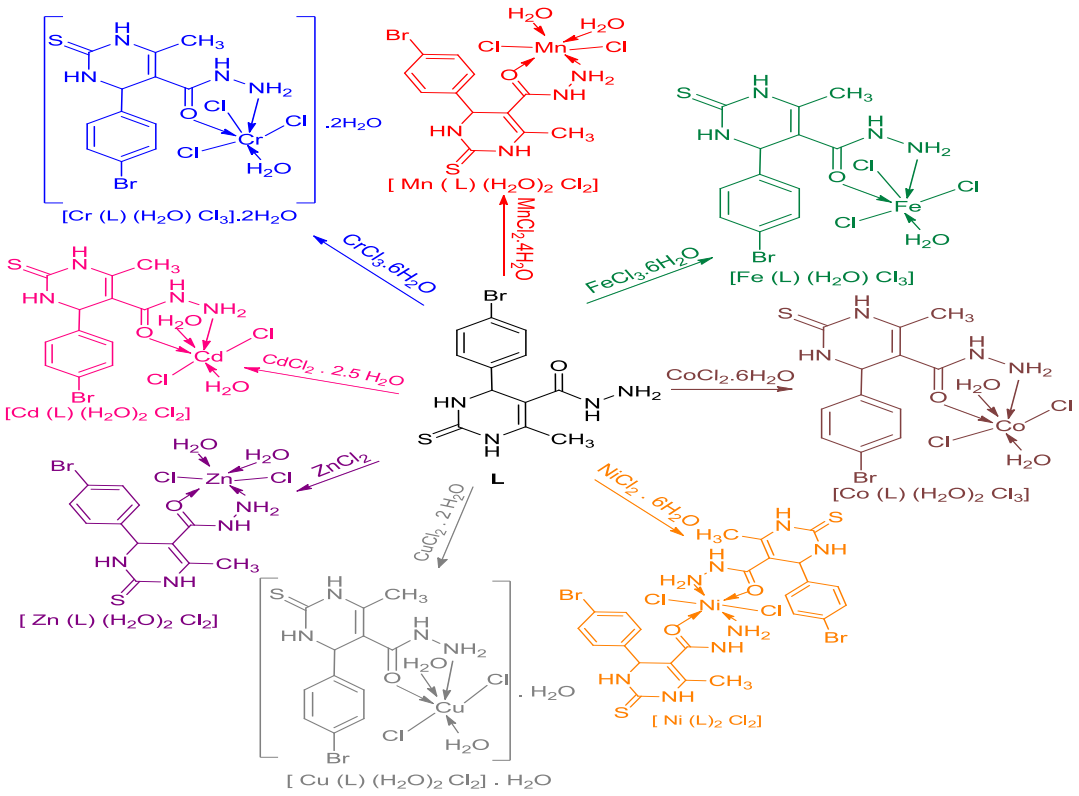

Scheme 2: Synthesis of metal Cr(III), Mn(II), Fe(III), Co(II), Ni(II), Cu(II), Zn(II), and Cd(II) Complexes.

Ligand (L): Yellow precipitate. Yield: 80%; M.p. 199 °C; FTIR (cm^{-1}) υ: 3314, 3168 (NH_2, NH), 2900 (C-H), 1661 (C=O), and 1279 (C=S). ^{1}H NMR (DMSO-d_6) δ: 2.30 (s, 3H, CH_3), 5.16 (s, 2H, NH_2), 5.17 (s, 1H, pyrimidine-H^4), 7.41 (d, 2H, *J* = 8.5 Hz, Ar-H), 7.65 (d, 1H, *J* = 8.5 Hz, Ar-H), 9.66 (s, 1H, NH), 10.37 (br, 1H, NH). ^{13}C NMR (DMSO-d_6) δ: 17.6 (CH_3), 60.2 (pyrimidine-C^4), 100.7 (pyrimidine-C^5), 121.3, 129.1, 131.9, 137.1, 144.9 (Ar-C, pyrimidine-C^6), 165.5 (C=O), 174.7 (C=S). UV–Vis (DMF), λ_{max} (nm): 233, 307. Elemental analysis for $C_{12}H_{13}BrN_4OS$: Found C=42.78, H=3.10, N=16.12, S=9.18. Calc. C=42.24, H=3.84, N=16.42, S=9.40.

Cr(III) complex: Yellow-green precipitate. Yield: 59%. M.p.: 247 °C. FTIR (cm^{-1}) υ: (3649-3335)br υ(H_2O), 3164, 3093 (NH_2, NH), 1636 (C=O), 644 (M-O), 551 (M=N), 416 (M=Cl). UV–Vis (DMF), λ_{max} (nm): 245, 341, 424. Elemental analysis for $CrC_{12}H_{19}BrCl_3N_4O_4S$: Found C=26.11, H=3.33, N=10.43, S=5.90. Calc. C=26.03, H=3.46, N=10.52, S=5.79.

Mn(II) complex: Light green precipitate. Yield: 70%. M.p.: 233 °C. FTIR (cm^{-1}) υ: (3446-3345)br υ(H_2O), 3224, 3169 (NH_2, NH), 1642 (C=O), 639 (M-O), 552 (M=N), 419 (M=Cl). UV–Vis (DMF), λ_{max} (nm): 284, 369, 584. Elemental analysis for $MnC_{12}H_{17}BrCl_2N_4O_3S$: Found C=28.09, H=3.70, N=11.93, S=6.10. Calc. C=28.65, H=3.41, N=11.41, S=6.37.

Fe(III) complex: gold precipitate. Yield: 85%. M.p.: 261 °C. FTIR (cm^{-1}) υ: (3423-3390)br υ(H_2O), 3230, 3117 (NH_2, NH), 1647 (C=O), 642 (M-O), 553 (M=N), 413 (M=Cl). UV–Vis (DMF), λ_{max} (nm): 241, 313, 496. Elemental analysis for $FeC_{12}H_{15}BrCl_3N_4O_2S$: Found C=27.03, H=3.74, N=2.12, S=10.89. Calc. C=27.64, H=2.90, N=10.74, S=6.15.

Co(II) Complex: Yellow precipitate. Yield: 76 %. M.p.: 270 °C. FTIR (cm^{-1}) υ: (3529-3473)br υ(H_2O), 3235, 3176 (NH_2, NH), 1626 (C=O), 640 (M-O), 580 (M=N), 417 (M=Cl). UV–Vis (DMF), λ_{max} (nm): 235, 310, 666. Elemental analysis for $CoC_{12}H_{17}BrCl_2N_4O_3S$: Found C=29.62, H=3.74, N=11.98, S=6.06. Calc. C=28.42, H=3.38, N=11.05, S=6.32.

Ni(II) Complex: Light green precipitate. Yield: 78%. M.p.: 295 °C. FTIR (cm^{-1}) υ: 3281, 3168 (NH_2, NH), 1646 (C=O), 609 (M-O), 515 (M-N), 405 (M-Cl). UV–Vis (DMF), λ_{max} (nm): 265, 348, and 417. Elemental analysis for $NiC_{24}H_{26}Br_2Cl_2N_8O_2S_2$: Found C=35.26, H=2.87, N=13.54, S=7.48. Calc. C=35.50, H=3.23, N=13.80, S=7.23.

Cu (II) Complex: Yellowish-green precipitate. Yield: 61%. M.p.: 286 °C. FTIR (cm^{-1}) υ: (3470-3365)br υ(H_2O), 3215, 3123 (NH_2, NH), 1650 (C=O), 633 (M-O), 549 (M-N), 414 (M-Cl). UV–Vis (DMF), λ_{max} (nm): 235, 314, 400. Elemental analysis for $CuC_{12}H_{20}BrCl_2N_4O_4S$: Found C=27.01, H=3.60, N=10.22, S=6.01. Calc. C=27.21, H=3.62, N=10.58, S=6.05.

Zn(II) Complex: Light yellow precipitate. Yield: 64%. M.p.: 216 °C. FTIR (cm^{-1}) υ: (3550-3314)br υ(H_2O), 3276, 3160 (NH_2, NH), 1623 (C=O), 625 (M-O), 516 (M-N), 412 (M-Cl). ^{1}H NMR (DMSO-d_6) δ: 2.29 (s, 3H, CH_3), 5.14 (s, 2H, NH_2), 5.15 (s, 1H, pyrimidine-H^4), 7.17 (d, 2H, *J* = 8.5 Hz, Ar-H), 7.72 (d, 1H, *J* = 8.5 Hz, Ar-H), 9.67 (s, 1H, NH), 10.39 (br, 1H, NH). ^{13}C NMR (DMSO-d_6) δ: 17.7 (CH_3), 60.1 (pyrimidine-C^4), 100.7 (pyrimidine-C^5), 121.3, 129.1, 131.9, 137.1, 145.9 (Ar-C, pyrimidine-C^6), 165.8 (C=O), 174.7 (C=S). UV–Vis (DMF), λ_{max} (nm): 233, 310. Elemental analysis for $ZnC_{13}H_{20}BrCl_2N_4O_3S$: Found C=29.90, H=3.05, N=10.50, S=6.43. Calc. C=29.54, H=3.81, N=10.60, S=6.07.

Cd(II) Complex: Light yellow precipitate. Yield: 83%. M.p.: 227 °C. FTIR (cm^{-1}) υ:(3500-3420)br υ(H_2O), 3263, 3117 (NH_2, NH), 1652 (C=O), 666 (M-O), 550 (M-N), 411 (M-Cl). ^{1}H NMR (DMSO-d_6) δ: 2.26 (s, 3H, CH_3), 5.12 (s, 2H, NH_2), 5.13 (s, 1H, pyrimidine-H^4), 7.10 (d, 2H, *J* = 8.5 Hz, Ar-H), 7.50 (d, 1H, *J* = 8.5 Hz, Ar-H), 9.65 (s, 1H, NH), 10.37 (br, 2H, 2NH). ^{13}C NMR (DMSO-d_6) δ: 17.6 (CH_3), 60.2 (pyrimidine-C^4), 100.5 (pyrimidine-C^5), 121.2, 129.1, 131.8, 137.2, 145.9 (Ar-C, pyrimidine-C^6), 165.9 (C=O), 174.7 (C=S). UV–Vis (DMF), λ_{max} (nm): 235, and 311. Elemental analysis for $CdC_{12}H_{17}BrCl_2N_4O_3S$: Found C=25.28, H=3, N=8.75, S=4.69. Calc. C=25.71, H=3.06, N=9.99, S=5.72.

Table 1. The physical properties of the ligand and complexes.

Compound	(m.w)	Colour	Yield %	M.P (°C)	Ω $^{-1}$ mol^{-1} cm^2	μeff (B.M)
Ligand ($C_{12}H_{13}BrN_4OS$)	341.23	pale yellow	80	150	5	-
[Cr (L) (H_2O) Cl_3].2H_2O	553.63	yellow green	59	247	2	3.73
[Mn(L)(H_2O)$_2$ Cl_2]	503.10	light green	70	233	9	5.60
[Fe (L)(H_2O) Cl_3]	521.45	gold	85	261	3	5.80
[Co (L)(H_2O)$_2$ Cl_2]	507.10	yellow	76	270	8	3.50
[Ni (L)$_2$ Cl_2]	812.05	light green	78	295	4	2.80
[Cu (L)(H_2O)$_2$ Cl_2]. H_2O	529.72	yellowish green	61	286	6	1.52
[Zn (L)(H_2O)$_2$ Cl_2]	528.58	Pale yellow	64	216	7	dia
[Cd (L) (H_2O)$_2$ Cl_2]	560.57	pale yellow	83	227	11	dia

2.5 In vitro antimicrobial

Antibacterial and antifungal properties were investigated using the disc diffusion method. The bacterial species include G^- (Escherichia *coli*) and G^+ (*Staphylococcus aureus*). *Candida albicans* and *Aspergillus flavus* are the used fungi. The strains used for the microorganisms are, ATCC11775, ATCC12600, ATCC 7102, and ATCC 9643 for *E. coil, S. aureus, Candida albicans*, and *Aspergillus flavus* respectively. The used negative control is DMSO. Ampicillin was used as a positive control for G^- bacteria and Kanamycin were used as a positive control for G^+ bacteria. Amphotericin B was used as a positive control for fungi.

3. Result and discussion

3.1 ^{1}HNMR

The ^{1}H NMR spectra of the hydrazide ligand **(L)**, the derived Cd(II), and Zn(II) complexes indicated the proposed assigned structure and completion of the complexation reaction. The ^{1}H NMR spectrum of the ligand showed the singlet signal at δ (2.30 ppm) for the methyl group at C^6 in the pyrimidine ring (33) and the singlet signal attributed to the NH_2 at δ (5.16 ppm) and the remaining pyrimidyl ring proton signal (H^4) at δ (5.17 ppm). The spectrum also revealed the signals assigned for the aryl proton signals in addition to the NH signals and the NH_2 peak. These latter signals have

been shown to undergo a shift to δ (5.16 ppm) in the afforded complexes at δ (5.12 ppm) and δ (5.14 ppm) for Cd(II) and Zn(II) complexes, respectively. The singlet signals of an amino group and NH protons of the ligand locate at δ (9.66 ppm) which have been shifted to δ (9.65 and 9.67 ppm) in Cd(II) and Zn(II) complexes, respectively, confirming the participation of NH_2 in chelation. The observed values assigned for the signals of the aryl protons are almost in the same position in the two complexes (minor shifts were observed).

3.2 ^{13}CNMR

At the normal temperature, ^{13}C NMR of **L**, Zn(II), and Cd(II) complexes was measured by using DMSO-d_6 as a solvent. The ligand displays signals at δ (17.6 ppm), δ (60.2 ppm), and δ (100.7 ppm). The first signal could be assigned to the CH_3 group. while the second signal could be belonging to the pyrimidine-C^4 and the third to pyrimidine-C^5. The aromatic carbon and pyrimidine-C^6 ligand created signals in the range of δ (121.3–144.9 ppm) (34). The signal at δ (174.7 ppm) corresponds to (C=S) (35). Furthermore, the signal δ (165.5 ppm) is created by the carbonyl group (36), which in Cd(II) and Zn(II) complexes appeared at δ (165.8 ppm) and δ (165.9 ppm), respectively. As a result of the oxygen lone pair's contribution to the metal's bond.

3.3 Elemental analysis

Elemental analysis of the ligand and its complexes data showed that the calculated and discovered percentages elemental a nalyses agree to a good degree. This supported the proposed structures of the ligand and complexes, complexes showed L: M molar ratios of 1:1 are Cr(III), Mn(II), Fe(III), Co(II), Cu(II), Zn(II), and Cd(II) complexes while Ni(II) complex is 1:2.

3.4 Molar conductivity

Molar conductivity data (Table 1). The ligand and complexes were dissolved in DMF to measure their conductivity and the obtained values were in the 2-11 Ω^{-1} cm^2 mol^{-1} range. These values indicate that it's are non-electrolytes and support the proposed structure that chlorides are within the inner coordination sphere.

3.4 FT-IR spectra

The infrared spectra of the ligand and its metal complexes showed many different bands in different regions that are displayed shapes in (Figure 2). The ligand showed two sharp bands in the region 3314 cm^{-1} and 3168 cm^{-1}, indicating vibrations of (NH_2 and NH) bonds respectively (37-39). Also showed a sharp band in 2900 cm^{-1} indicating the vibration of the (C-H) aliphatic bond (40). The carbonyl group (C=O) of the ligand showed a sharp and long vibration band at 1661 cm^{-1} (41). while thione group (C=S) appeared 1279 cm^{-1} (42). In the metal complexes case, the vibrations of some groups that were bonded with the metal ions showed shifted to lower values, and the vibration band of some other groups remained at the same value or at less shifted because they were not bonded with metals ions or because they were far from the bonding regions. In addition, some complexes showed new vibrational bands for their bonding with water molecules and chloride ions. Vibration bands of the amine group appeared in Cr(III), Mn(II), Fe(III), Co(II), Ni(II), Cu(II), Zn(II), and Cd(II) complexes in the regions 3164, 3224, 3230, 3235, 3281, 3215, 3276, and 3263 cm^{-1} respectively (43). We note that they are lower than what this group appeared in the ligand, indicating its bond with the metal ion. in the other hand, the vibration bands of the carbonyl group appeared in Cr(III), Mn(II), Fe(III), Co(II), Ni(II), Cu(II), Zn(II) and Cd(II) complexes also in the regions 1636, 1642, 1647, 1626, 1646, 1650,1623, and 1652 cm^{-1} respectively (43). These values indicate bonded metal ions with the carbonyl group (36).

3.5 Electronic spectra and magnetic moment measurements

The UV-visible of the DMF solution of ligand and its complexes were measured. The L has the band at 233 nm (44) indication of the electronic transition of $\pi \rightarrow \pi^*$ and the band at 307 nm indication for the electronic transition of n $\rightarrow \pi *$ (45) as listed in Table 2, these values in the metal complexes have a shift due to the coordination of the ligand with the metal (Figure3). Cr(III) complex showed the value of 3.73 Bohr Magnetons (B.M.) representing the presence of three unpaired electrons of the octahedral Cr(III) which have three broad bands appear at 245 nm $\pi \rightarrow \pi *$, 341 nm n $\rightarrow \pi^*$ and 424 nm for ^4A_2g (F) $\rightarrow$ ^4T_2g(F) transition (46). Mn (II) complex showed μ_{eff} value of 5.60 indicating a high spin octahedral geometry and showed bands at 284 nm $\pi \rightarrow \pi *$, 369 nm n $\rightarrow \pi *$, and 584 nm for ^6A_1g(S) $\rightarrow$ ^4T_1g(G) transition (47, 48). Fe(III) Complex showed μ_{eff} value of 5.80 indicating octahedral geometry and showed bands at 241 nm $\pi \rightarrow \pi *$, 313 nm n $\rightarrow \pi *$, and 496 nm for ^6T_1g(D) $\rightarrow$ ^6A_1g transition (46). The μ_{eff} value of Co (II) Complex is 3.50 refers a high spin octahedral geometry and UV-visible spectroscopy showed two sharp bands at 235

nm $\pi \rightarrow \pi*$, 310 nm n $\rightarrow \pi*$ and a broad band at 666 nm for $^4T_1g(F) \rightarrow {}^4T_2g(F)$ transition (48). The magnetic moment of the Ni(II) complex is 2.80 B.M which indicates octahedral geometry (49, 50), this complex shows three absorption spectra bands at 265 nm $\pi \rightarrow \pi*$, 348 nm n $\rightarrow \pi*$, and 417 nm for $^3A_2g_{(F)} \rightarrow {}^3T_1g_{(F)}$ transition (51). The Cu (II) complex magnetic moment is 1.52 B.M which indicate tetragonally distorted octahedral (37). Cu (II) complex shows two sharp bands at 235 nm $\pi \rightarrow \pi*$, 314 nm n $\rightarrow \pi*$ and a broad band at 400 nm for $^2B_1 \rightarrow {}^2E$ transition (52). Zn (II) and Cd (II) Complexes are diamagnetic. Zn(II) complex showed two bands at 233 nm $\pi \rightarrow \pi*$ and 310 nm n $\rightarrow \pi*$ (49). Cd (II) Complex appeared two bands at 286 nm $\pi \rightarrow \pi*$ and 311 nm n $\rightarrow \pi*$ (52).

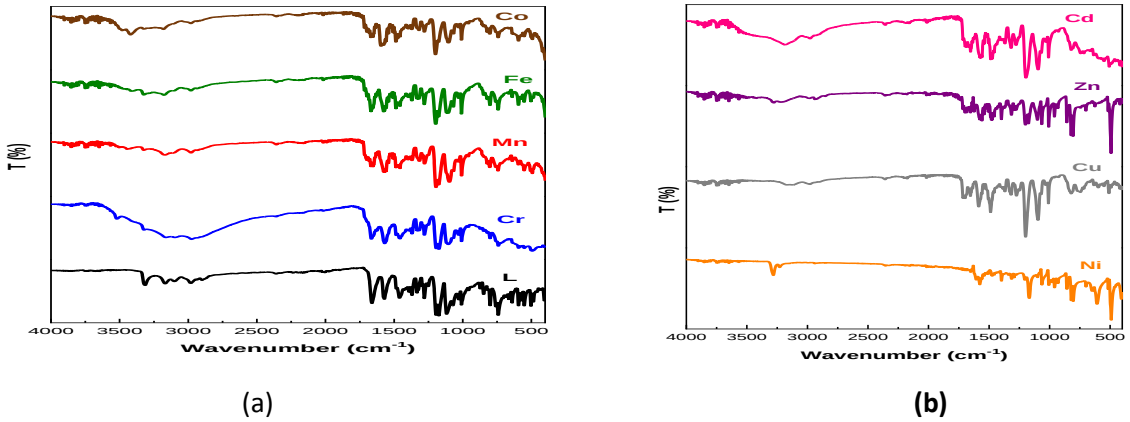

Figure 2. FT-IR spectrum (a) of ligand, Cr(III), Mn(II), Fe(III), and Co(II) complexes and (b) of Ni(II), Cu(II), Zn(II), and Cd(II) complexes.

Table 2. UV-Vis Analysis

Compound	λ_{max} (nm)	λ_{max} (cm^{-1})	Electronic transition
L $C_{12}H_{13}BrN_4OS$	233 307	42918 32573	$\pi \rightarrow \pi^*$ n $\rightarrow \pi^*$
[Cr (L) (H_2O) Cl_3].$2H_2O$	245 341 424	40816 29325 23584	$\pi \rightarrow \pi^*$ n$\rightarrow \pi^*$ ^4A_2g (F) $\rightarrow {}^4T_2g$(F)
[Mn(L)$(H_2O)_2$ Cl_2]	284 369 584	35211 27100 17123	$\pi \rightarrow \pi^*$ n$\rightarrow \pi^*$ $^6A_1g(S) \rightarrow {}^4T_1g(G)$
[Fe (L)(H_2O) Cl_3]	241 313 496	41493 31948 20161	$\pi \rightarrow \pi^*$ n$\rightarrow \pi^*$ $^6T_1g(D) \rightarrow {}^6A_1g$
[Co (L)$(H_2O)_2$ Cl_2]	235 310 666	42553 32258 15015	$\pi \rightarrow \pi^*$ n$\rightarrow \pi^*$ $^4T_1g(F) \rightarrow {}^4T_2g(F)$
[Ni $(L)_2$ Cl_2]	265 348 417	37735 28735 23980	$\pi \rightarrow \pi^*$ n $\rightarrow \pi^*$ $^3A_2g_{(F)} \rightarrow {}^3T_1g_{(F)}$
[Cu (L)$(H_2O)_2$ Cl_2]. H_2O	235 314 400	42553 31847 25000	$\pi \rightarrow \pi^*$ n $\rightarrow \pi^*$ $^2B_1 \rightarrow {}^2E$
[Zn (L)$(H_2O)_2$ Cl_2]	233 310	42918 32258	$\pi \rightarrow \pi^*$ n $\rightarrow \pi^*$
[Cd (L) $(H_2O)_2$ Cl_2]	235 311	42553 32154	$\pi \rightarrow \pi^*$ n $\rightarrow \pi^*$

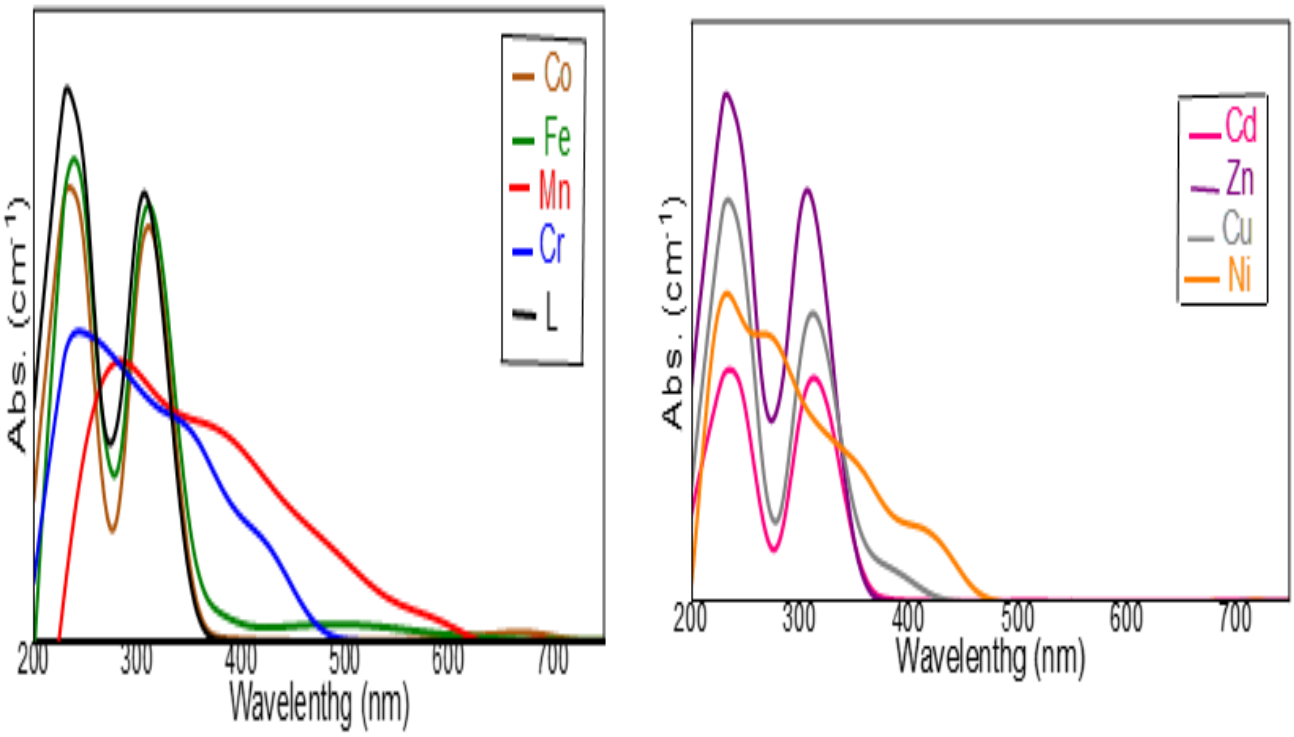

(a) (b)

Figure 3. UV-Vis spectrum (a) of ligand, Cr(III), Mn(II), Fe(III) and Co(II) complexes and (b) of Ni(II), Cu(II), Zn(II), and Cd(II) complexes.

3.6 Thermal analysis

The TGA and DTA As shown in (Table 3), the temperature range measuring is from room temperature to 477 °C. Cr(III)complex emphasized that were thermally stable up to 87 °C loss of one molecule of hydration water and Cu(II) complex at 90 °C loss of one molecule of hydration water, loss of two molecules of coordination water of Cr(III), Mn(II), Fe(III), Co(II), Cu(II), Zn(II), and Cd(II) complexes at 124, 176, 131, 147, 190, 127, and 137 °C respectively. Chlorides are lost in all complexes at a range between 125-284 °C. Finally, the decomposition and formation of metal oxides of complexes range between 228– 470 °C.

3.7 XRD

As shown in (Figure 4) all complexes are crystallized, The monocrystalline X-ray diffraction data for the complexes crystal system according to (Table 4) shows **L** is cubic. Cr(II), Mn(II), Co(II), and Ni(II) are monoclinic while Fe(III) and Zn(II) complexes are hexagonal**,** Cu(II) complex is orthorhombic and Cd(II) complex is tetragonal.

Table 3. Thermal data of the metal complexes.

Compound	Temp. Range (°C)	DTA (Peak)		TGA (wt. loss%)		Assignment
		Endo	Exo.	Calc.	Found	
[Cr (L) (H_2O) Cl_3] .2H_2O	29 – 87	Endo	-	6.50	6.30	Loss of two hydrated H_2O
	88 -124	Endo	-	3.20	3.00	Loss of one coordinated H_2O
	125 - 264	-	Exo.	19.2	19.00	Loss of three Cl
	265 – 430		- Exo.	61.60	61.80	Decomposition of the complex forming Cr_2O_3
[Mn(L)(H_2O)$_2$ Cl_2]	26 – 176	Endo	-	7.10	7.00	Loss of two coordinated H_2O
	177 -253	Endo	-	14.11	14.40	Loss of two Cl
	254 - 418	-	Exo.	67.80	67.20	Decomposition of the complex forming MnO
[Fe (L)(H_2O) Cl_3]	25 – 131	Endo	-	3.40	2.10	Loss of one coordinated H_2O
	132 – 266	Endo	-	20.40	20.00	Loss of three Cl
	267 – 440	-	Exo.	65.40	65.20	Decomposition of the complex forming Fe_2O_3
[Co (L)(H_2O)$_2$ Cl_2]	29 – 147	Endo	-	7.10	6.90	Loss of two coordinated H_2O
	148 – 265	-	Exo.	14.00	13.90	Loss of two Cl
	266 – 403	Endo	-	67.30	67.10	Decomposition of the complex forming CoO
[Ni (L)$_2$ Cl_2]	25 – 227	Endo	-	8.70	8.30	Loss of two Cl
	228 –477	-	Exo.	84.50	84.34	Decomposition of the complex forming NiO
[Cu (L)(H_2O)$_2$ Cl_2]. H_2O	27 – 90	Endo	-	3.40	2.30	Loss of one hydrated H_2O
	91 – 190	-	Exo.	6.80	6.20	Loss of two coordinated H_2O
	191 – 284	Endo	-	13.40	14.10	Loss of two Cl
	285 - 456	-	Exo.	64.01	64.0	Decomposition of the complex forming CuO
[Zn (L)(H_2O)$_2$ Cl_2]	26-127	Endo	-	6.80	6.20	Loss of two coordinated H_2O
	128 – 227	Endo	-	13.43	13.20	Loss of two Cl
	228 – 416	-	Exo.	64.50	64.30	Decomposition of the complex forming ZnO
[Cd (L) (H_2O)$_2$ Cl_2]	25 – 137	Endo	-	6.40	6.20	Loss of two coordinated H_2O
	138 – 281	Endo	-	12.66	12.20	Loss of two Cl
	282 - 470	-	Exo.	60.90	60.40	Decomposition of the complex forming CdO

Table 4. XRD Analysis

Comp.	Crystal system	Space group	a (A°)	b (A°)	c (A°)	α	β	γ	Crystallite size (nm)	Volume $(A°)^3$
L	cubic	Pm-3m	6.11	6.11	6.11	90	90	90	28.9	228.09
Cr (III) complex	monoclinic	C12/c1	12.04	6.84	11.65	90	94.07	90	2.06	956.99
Mn (II) complex	monoclinic	C12/c1	7.41	8.80	3.68	90	98	90	10.3	237.63
Fe (III) complex	hexagonal	$P6_3$	17.67	17.67	9.24	90	90	120	13.1	2498.48
Co (II) complex	monoclinic	C12/m1	7.28	8.54	3.57	90	97.55	90	40	220.03
Ni (II) complex	monoclinic	P12/m1	6.90	6.88	8.80	90	92.09	90	15.1	417.47
Cu (II) complex	orthorhombic	Pbam	7.41	8.09	3.74	90	90	90	8.2	224.20
Zn (II) complex	hexagonal	$P6_3/m$	10.56	10.56	3.73	90	90	120	33.3	360.22
Cd (II) complex	tetragonal	P-42m	5.86	5.86	5.72	90	90	90	1.1	196.42

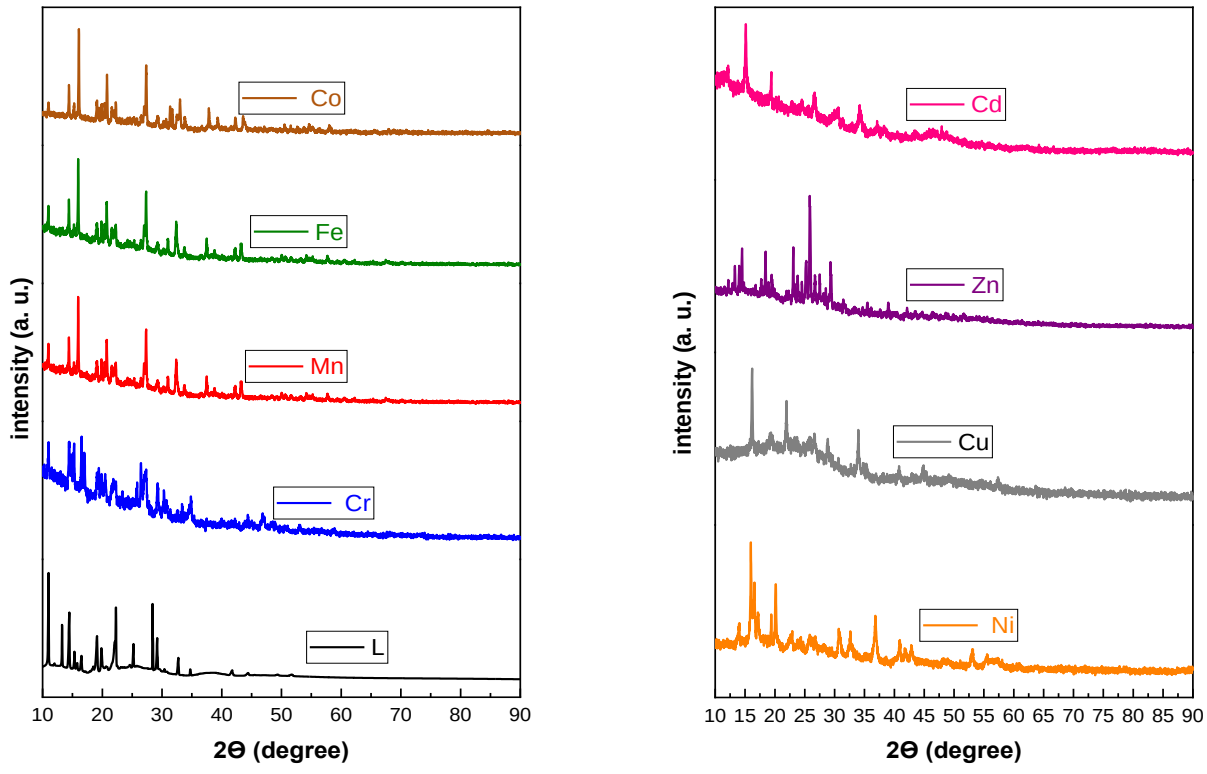

(a) (b)

Figure 4. XRD Pattern of (a) the ligand, Cr(III), Mn(II), Fe(III), and Co(II) complexes, (b) Ni(II), Cu(II), Zn(II) and Cd(II) complexes

3.8 Transmission electron microscopy (TEM)

As shown in (Figure 5) ligand TEM investigation showed that it has a particle size ranging from 21-29 nm. The Co(II) complex showed particle size ranging from 21-40 nm. The Mn(II) complex showed particle size ranging from 9-14 nm, Ni(II) showed particle size ranging from 27-14 nm, while Zn(II) complexes showed particle size ranging from 27-34. The TEM result supports the data XRD analysis.

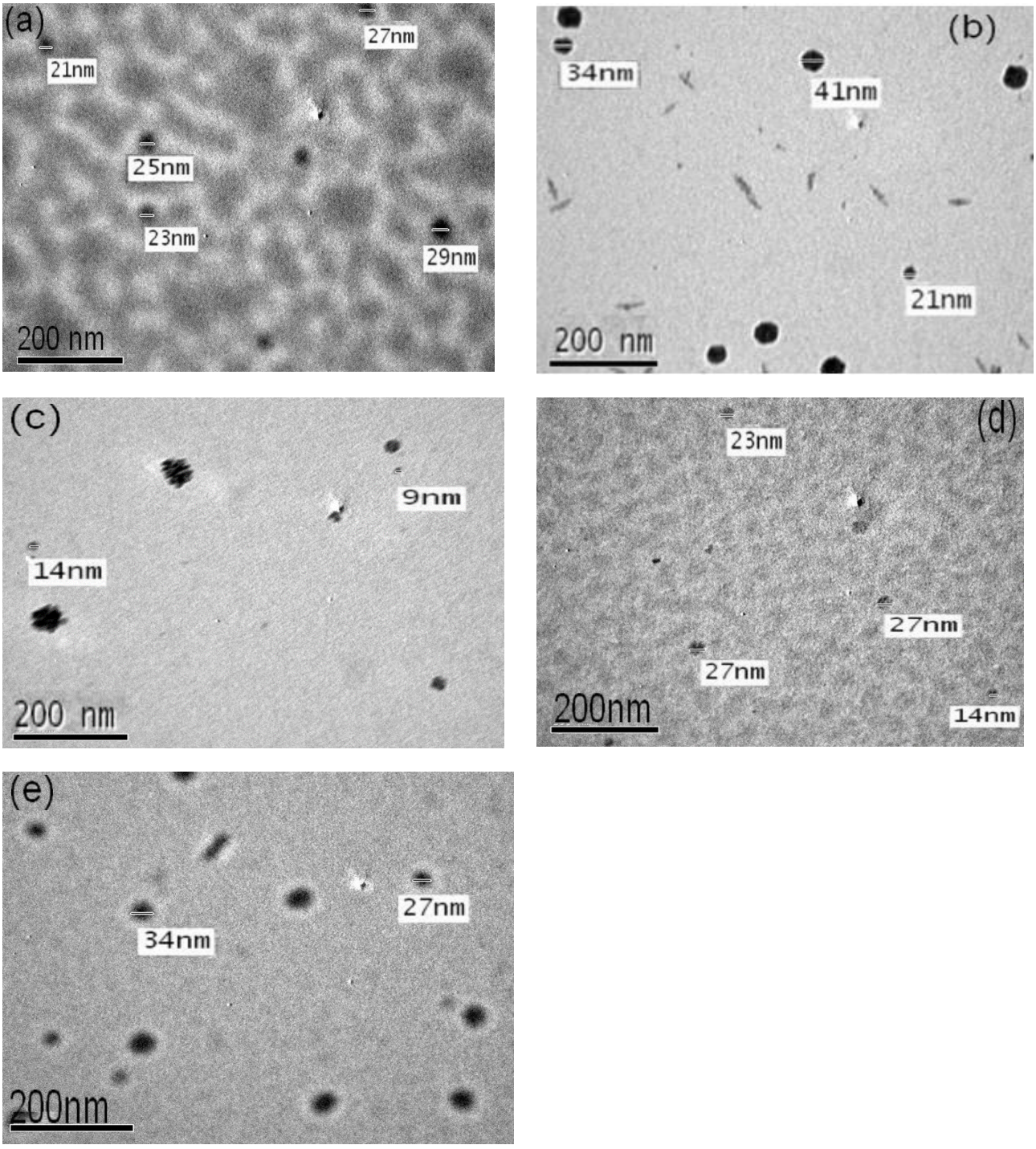

Figure 5. TEM images of (a) ligand, (b) Co(II) complex, (c) Mn(II) complex, and (d) Ni(II) complex (e) Zn(II) complex.

3.9 Antimicrobial

The antimicrobial activity data are summarized in (Table 5) and (Figure 6,7). The antibacterial and antifungal activities test was applied to the ligand and complexes against two bacterial strains it is *E. coli* and *S. aureus*. Also, against two fungal strains, it is *Candida albicans* and *Aspergillus flavus*. The highest antibacterial and antifungal was the Cd (II) complex (Table 5), followed by the Co (II) and Ni (II) complex which gave results against the two kinds of bacteria and *Candida albicans* fungus. The Zn (II) complex gave high activity against the two kinds of bacteria while did not give any activity against the fungi. The difference in the antimicrobial activity of the metal complexes may depend on the cell permeability. Ligand activity has lower than that of complexes. This could be understood by Tweedy's chelation theory and Overtone's concept (related to cell permeability). Upon chelation, the metal polarity is diminished as a result of the partial distribution of their positive charge with ONS donor atoms and π-electron delocalization throughout the entire chelating ring. So, this chelation increases the metal lipophilicity to penetrate the lipid membrane of the bacteria by blocking the enzymes binding sites in the microorganism by the metal complex. Also, these metal complexes disturb the respiration process of the microorganism cell by blocking the protein synthesis essential for growth. The ligand and metal complexes' activity variation depends on the permeability of the cell membrane or the differences in the ribosomes of microbial cells. On the other hand, the ligand donor atoms may inhibit the microorganism enzyme activity, these groups are required for their activity, and appear to be especially more sensitive, and this disturbed and deactivation by the metal ions upon chelation (53).

Table 5. The Antimicrobial test of the ligand and its metal complexes.

Sample			Inhibition zone diameter (mm / mg sample)			
			Bacterial species		Fungal species	
			G^+	G^-		
			Staphylococcus aureus	Escherichia coli	Aspergillus flavus	Candida albicans
Standard	Antibacterial agent	Ampicillin	---	25	---	---
		Kanamycin	27	---	---	---
	Amphotericin B Antifungal agent		---	---	17	21
Control: DMSO			0.0	0.0	0.0	0.0
L			14.67	10.33	0.0	0.0
Cr (III) complex			15	14	0.0	0.0
Mn (II) complex			13.67	10.33	0.0	0.0
Fe (III) complex			20	17.67	0.0	0.0
Co (II) complex			25	19.33	0.0	20.67
Ni (II) complex			26	17	0.0	25
Cu (II) complex			18.33	17.67	0.0	0.0
Zn (II) complex			27	24	0.0	0.0
Cd (II) complex			34	19	36	30

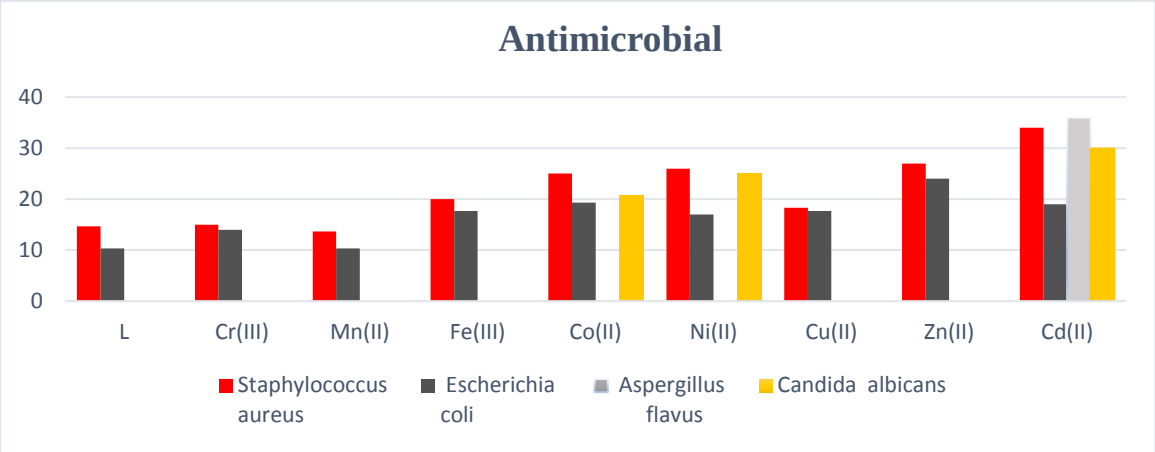

Figure. 6 Antimicrobial effects of the L and its M-Complexes.

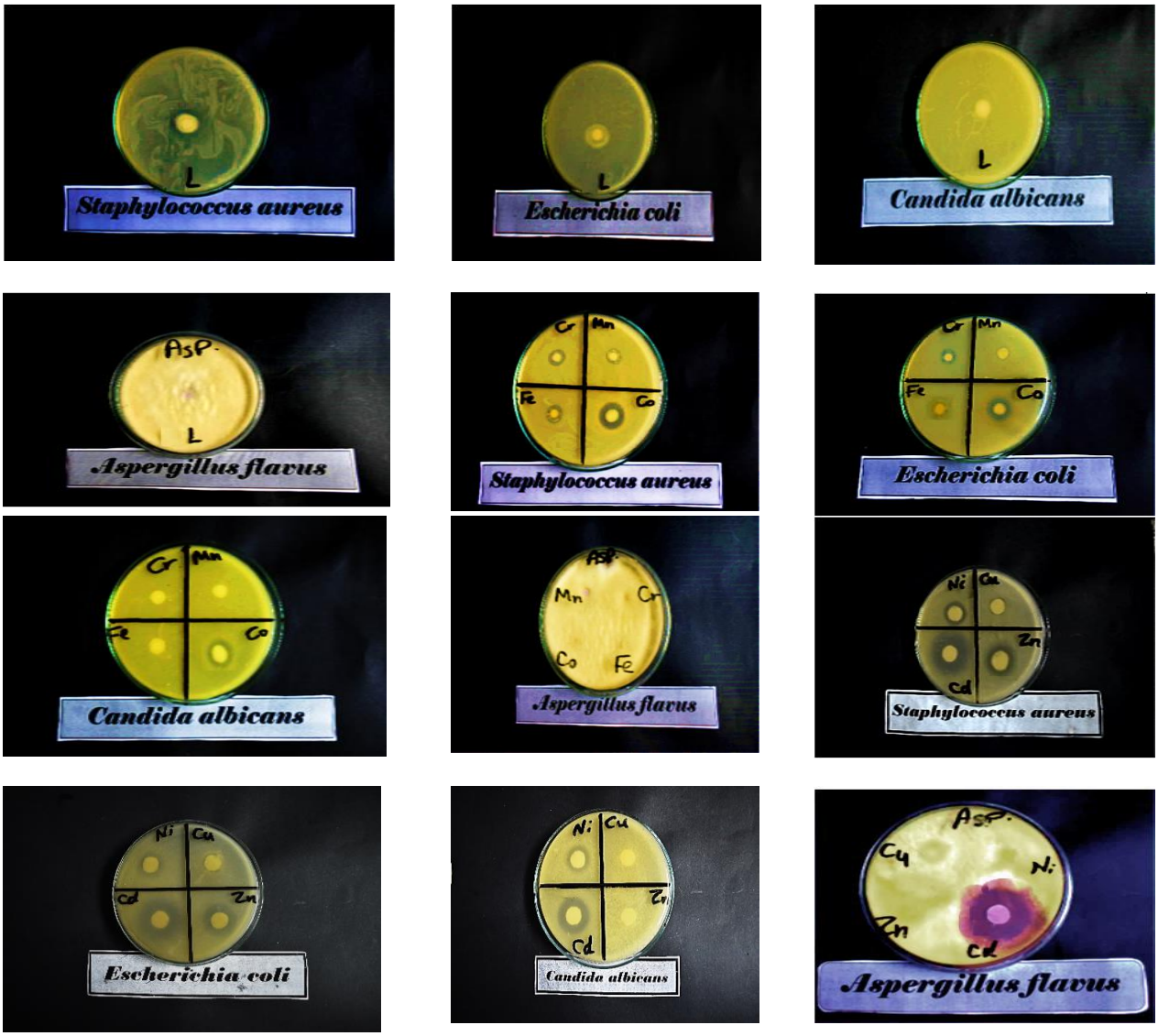

Figure 7. Inhibition zone diameter of antibacterial of ligand and its complexes.

4. Conclusion

A new 4-(4-bromophenyl)-6-methyl-2-thioxo-1,2,3,4-tetrahydropyrimidine-5-carbohydrazide ligand; Its Cr(III), Mn(II), Fe(III), Co(II), Ni(II), Cu(II), Zn(II) and Cd(II) metal complexes have been synthesized and characterized via elemental analysis, XRD, UV–Vis, IR, TGA, DTA, NMR, and TEM. The ligand acts as neutral bidentate and is coordinated via the oxygen atom of the carbonyl group and the terminal nitrogen atom of hydrazide moiety. The conductivity measurements showed that all the complexes are nonelectrolytes. The magnetic susceptibility of Cr(III), Mn(II), Fe(III), Co(II), Ni(II), and Cu(II) complexes showed 3.73, 5.60, 5.80, 3.50, 2.80, and 1.52 B.M respectively. Cd(II) complex showed the highest antimicrobial against *Staphylococcus aureus, Escherichia coli,* and *Candida albicans*. All compounds didn't show any activity against *Aspergillus flavus* except Cd(II) complex gave a high activity.

5. Conflicts of interest

"There are no conflicts to declare".

6. References

1.Karami K, Jamshidian N, Zakariazadeh M, Momtazi-Borojeni AA, Abdollahi E, Amirghofran Z, et al. Experimental and theoretical studies of Palladium-hydrazide complexes' interaction with DNA and BSA, in vitro cytotoxicity activity and plasmid cleavage ability. Computational Biology and Chemistry. 2021;91:107435.

2.AL-FAKEH MS, AMIRI N, AL-HAKEMI AN, SAEED SE-S, ALBADRI AE. AJ Csian OURNALOF HEMISTRY AJ Csian OURNALOF HEMISTRY. Asian Journal of Chemistry. 2020;32(10):2502-6.

3.Abdelsalaam H, Zayed EM, Zayed MA, Nouman M. Synthesis, structural characterization, thermal behaviour and antimicrobial activity of copper, cadmium and zinc chelates of traizole-thiole ligand in comparison with theoretical molecular orbital calculations. Egyptian Journal of Chemistry. 2019;62(Special Issue (Part 1) Innovation in Chemistry):145-63.

4.Zayed EM. New ligand metal complexes study: synthesis, spectroscopic, DFT, and docking studies, and molecular structure. Egyptian Journal of Chemistry. 2022;65(9):281-91.

5.Alhakimi AN, Alnawmasi TAAJS, Saeed SE-S, Alhamzi EH. Synthesis, Spectroscopic Characterization, and Anticancer Activity of Metal Complexes with a Novel Schiff Base Ligand from B-Diketone Derivatives. Journal of The Chemical Society of Pakistan. 2022;44(6):596.

6.Wang N, Świtalska M, Wang L, Shaban E, Hossain MI, El Sayed IET, et al. Structural Modifications of Nature-Inspired Indoloquinolines: A Mini Review of Their Potential Antiproliferative Activity. Molecules. 2019;24(11):2121.

7.El-Sayed SS, Alhakimi AN. Synthesis, characterization of Lanthanum mixed ligand complexes based on benzimidazole derivative and the effect of the added ligand on the antimicrobial, and anticancer activities. Journal of Qassim University for Science. 2022;15:35-53.

8.Shama SA, El-Molla MM, Basalah RF, Saeed SE-S. Fading Time Study on Prepared Thymolphthalein, Phenolphthalein and their Mixture Disappearing Ink. Research Journal of Textile and Apparel. 2008;12(1):9-18.

9.El- Molla MM, Shama SA, El- Sayed Saeed S. Preparation of disappearing inks and studying the fading time on different paper surfaces. Journal of forensic sciences. 2013;58(1):188-94.

10.Nawwar GAM, Zaher KSA, Shaban E, El-Ebiary NMA. Utilizing Semi-Natural Antibacterial Cellulose to Prepare Safe Azo Disperse Dyes and Their Application in Textile Printing. Fibers and Polymers. 2020;21(6):1293-9.

11.Shaban E, Świtalska M, Wang L, Wang N, Xiu F, Hayashi I, et al. Synthesis and In Vitro Antiproliferative Activity of 11-Substituted Neocryptolepines with a Branched ω-Aminoalkylamino Chain. Molecules. 2017;22(11):1954.

12.Hussain MMM, Bhat KI, Revanasiddappa B, Bharthi D. Synthesis and biological evaluation of some novel 2-mercapto pyrimidines. International Journal of Pharmacy and Pharmaceutical Sciences. 2013;5(2):471-3.

13.Mohamed MS, Awad SM, Zohny YM, Mohamed ZM. New theopyrimidine derivatives of expected antiinflammatory activity. Pharmacophore. 2012;3(1):62-75.

14.Nag S, Pathak R, Kumar M, Shukla P, Batra S. Synthesis and antibacterial evaluation of ureides of Baylis–Hillman derivatives. Bioorganic & medicinal chemistry letters. 2006;16(14):3824-8.

15.Hoffmann H-H, Kunz A, Simon VA, Palese P, Shaw ML. Broad-spectrum antiviral that interferes with de novo pyrimidine biosynthesis. Proceedings of the National Academy of Sciences. 2011;108(14):5777-82.

16.Clercq ED, Holý A. Acyclic nucleoside phosphonates: a key class of antiviral drugs. Nature Reviews Drug Discovery. 2005;4(11):928-40.

17.Trivedi AR, Dodiya DK, Ravat NR, Shah VH. Synthesis and biological evaluation of some new pyrimidines via a novel chalcone series. Arkivoc. 2008;11:131-41.

18.Trivedi AR, Siddiqui AB, Shah VH. Design, synthesis, characterization and antitubercular activity of some 2-heterocycle-substituted phenothiazines. Arkivoc. 2008;2:210-7.

19.Agarwal A, Srivastava K, Puri S, Chauhan PM. Synthesis of 2, 4, 6-trisubstituted pyrimidines as antimalarial agents. Bioorganic & medicinal chemistry. 2005;13(15):4645-50.
20.Agarwal A, Srivastava K, Puri S, Sinha S, Chauhan PM. A small library of trisubstituted pyrimidines as antimalarial and antitubercular agents. Bioorganic & medicinal chemistry letters. 2005;15(23):5218-21.
21.Helal TA, Mohsein HF, Obaid NH. Synthesis with Spectral Investigation of New Ligand Derived From Pyrimidine with Some Metal Complexes. Journal of International Pharmaceutical Research. 2019:6-13.
22.Balkan A, Ertan M, Burgemeister T. Synthesis and Structural Evaluations of Thiazolo [3, 2- a] pyrimidine Derivatives. Archiv der Pharmazie. 1992;325(8):499-501.
23.Akbari J, Kachhadia P, Tala S, Bapodra A, Dhaduk M, Joshi H, et al. Synthesis of some new 1, 2, 3, 4-tetrahydropyrimidine-2-thiones and their thiazolo [3, 2-a] pyrimidine derivatives as potential biological agents. Phosphorus, Sulfur, and Silicon and the Related Elements. 2008;183(8):1911-22.
24.Weinhardt K, Wallach MB, Marx M. Synthesis and antidepressant profiles of phenyl-substituted 2-amino- and 2-[(alkoxycarbonyl) amino]-1, 4, 5, 6-tetrahydropyrimidines. Journal of medicinal chemistry. 1985;28(6):694-8.
25.Mohan J, Chadha V, Chaudhary H, Sharma B, Pujari H. Heterocyclic systems containing bridgehead nitrogen atom. 13. Antifungal and antibacterial activities of thiazole and thiazolidinone derivatives. Indian J Exp Biol. 1972(10 (1)):37-40.
26.Pandey S, Pandey P, Singh J. Synthesis, characterization and fungicidal activity of N-(5-oxo-3, 7-diaryl-6, 7-dihydro-5H-thiazolo [3, 2, a] pyrimidin-6-yl) benzamide derivatives. Der Pharma Chemica. 2014;6(1):170-5.
27.Pandey S, Pandey P, Gautam SS, Singh J. Synthesis, characterization and antifungal evaluation of substituted pyrimidin-2-thione derivatives. Research Journal of Pharmacy and Technology. 2021;14(1):275-9.
28.Alkhamis K, Alkhatib F, Alsoliemy A, Alrefaei AF, Katouah HA, Osman HE, et al. Elucidation for coordination features of hydrazide ligand under influence of variable anions in bivalent transition metal salts; green synthesis, biological activity confirmed by in-silico approaches. Journal of Molecular Structure. 2021;1238:130410.
29.Shakdofa MM, Morsy NA, Rasras AJ, Al- Hakimi AN, Shakdofa AM. Synthesis, characterization, and density functional theory studies of hydrazone–oxime ligand derived from 2, 4, 6- trichlorophenyl hydrazine and its metal complexes searching for new antimicrobial drugs. Applied Organometallic Chemistry. 2021;35(2):e6111.
30.Sawant RL, Wadekar JB, Kharat SB, Makasare HS. Targeting PPAR-γ to design and synthesize antidiabetic thiazolidines. EXCLI journal. 2018;17:598.
31.Younis A, Awad G. Utilization of Ultrasonic as an Approach of Green Chemistry for Synthesis of Hydrazones and Bishydrazones as Potential Antimicrobial Agents. Egyptian Journal of Chemistry. 2020;63(2):599-610.
32.Gawrońska-Grzywacz M, Piątkowska-Chmiel I, Popiołek Ł, Herbet M, Dudka J. The N-Substituted-4-Methylbenzenesulphonyl Hydrazone Inhibits Angiogenesis in Zebrafish Tg (fli1: EGFP) Model. Pharmaceuticals. 2022;15(11):1308.
33.Neamah R, Adnan S. Synthesis, Characterization, and Study the Biological Activity for ShiffBase and β-lactam Derivatives from 2-amino-4-hydroxy-6-methyl pyrimidine. 2021;12(3):229-33.
34.Georgiades SN, Nicolaou PG, Panagiotou N. N-Directed Pd-Catalyzed Photoredox-Mediated C–H Arylation for Accessing Phenyl-Extended Analogues of Biginelli/Suzuki-Derived Ethyl 4-Methyl-2, 6-diphenylpyrimidine-5-carboxylates. Catalysts. 2021;11(9):1071.
35.Mohammed S, Moustafa A, Ahmed N, El-Sayed H, Mohamed A. Nano-K2CO3-Catalyzed Biginelli-Type Reaction: Regioselective Synthesis, DFT Study, and Antimicrobial Activity of 4-Aryl-6-methyl-5-phenyl-3, 4-dihydropyrimidine-2 (1H)-thiones. Russian Journal of Organic Chemistry. 2022;58(1):136-43.
36.Alhakimi AN, Shakdofa MM, Saeed S, Shakdofa AM, Al-Fakeh MS, Abdu AM, et al. Transition Metal Complexes Derived From 2-hydroxy-4-(p-tolyldiazenyl) benzylidene)-2-(p-tolylamino) acetohydrazide Synthesis, Structural Characterization, and Biological Activities. Journal of the Korean Chemical Society. 2021;65(2):93-105.
37.Alhakimi AN. Synthesis, Characterization and Microbicides Activities of N-(hydroxy-4-((4-nitrophenyl) diazenyl) benzylidene)-2-(phenylamino) Acetohydrazide Metal Complexes. Egyptian Journal of Chemistry. 2020;63(4):1509-25.
38.Saeed SE-S, Al-Harbi TM, Alhakimi AN, Abd El-Hady M. Synthesis and Characterization of Metal Complexes Based on Aniline Derivative Schiff Base for Antimicrobial Applications and UV Protection of a Modified Cotton Fabric. Coatings. 2022;12(8):1181.
39.El- Sayed Saeed S, Alharbi TM, Abdel- Mottaleb M, Al- Hakimi AN, Albadria AE, Abd El- Hady M. Novel Schiff base transition metal complexes for imparting UV protecting and antibacterial cellulose fabric: Experimental and computational investigations. Applied Organometallic Chemistry. 2022:e6889.
40.Han Mİ, Atalay P, İmamoğlu N, Küçükgüzel ŞG. Synthesis, characterization and anticancer activity of novel hydrazide-hydrazones derived from ethyl paraben. J Res Pharm. 2020;24(3):341-9.

41.Aroua LM, Al-Hakimi AN, Abdulghani MA, Alhag SK. Cytotoxic urea Schiff base complexes for multidrug discovery as anticancer activity and low in vivo oral assessing toxicity. Arabian Journal of Chemistry. 2022;15(8):103986.
42.BÜYÜKKIDAN B, BÜYÜKKIDAN N, Aslı A. NEW SCHIFF BASES DERIVED from 3, 4-DIAMINO-1H-1, 2, 4-TRIAZOLE-5 (4H)-THIONE: SYNTHESIS and CHARACTERIZATION. Journal of Scientific Reports-A. 2022;2687(048):25-41.
43.KOÇ HC, ATLIHAN İ, MEGA-TİBER P, ORUN O, KÜÇÜKGÜZEL ŞG. Synthesis of some novel hydrazide-hydrazones derived from etodolac as potential anti-prostate cancer agents. 2022;26(1):1-12.
44.Sultana US, Habib MA, Amin MK, Mahiuddin M, Zahan MK-E-, Islam ABMN. Synthesis, Structural Properties of Hydrazine Carbodithioate Schiff Base and Their Metal Complexes and Evaluation of Their Biological Activity. Egyptian Journal of Chemistry. 2020;63(10):3811-6.
45.Lakma A, Pradhan RN, Hossain SM, van Leusen J, Kögerler P, Singh AK. Synthesis, structure and magnetic properties of Ni (II) and Cu (II),[2× 2] grid complexes of pyrimidine-based symmetric ditopic ligands. Inorganica Chimica Acta. 2019;486:88-94.
46.Alorini TA, Al-Hakimi AN, Saeed SE-S, Alhamzi EHL, Albadri AE. Synthesis, characterization, and anticancer activity of some metal complexes with a new Schiff base ligand. Arabian Journal of Chemistry. 2022;15(2):103559.
47.Palmer S, Reddy BJ, Frost RL. Application of UV–Vis, near-infrared and mid-infrared spectroscopy to the study of Mn-bearing humites. Polyhedron. 2007;26(2):524-33.
48.Al-Hakimi AN, Shakdofa MM, El-Seidy A, El-Tabl AS. Synthesis, Spectroscopic, and Biological Studies of Chromium (III), Manganese (II), Iron (III), Cobalt (II), Nickel (II), Copper (II), Ruthenium (III), and Zirconyl (II) Complexes of N 1, N 2-Bis (3-((3-hydroxynaphthalen-2-yl) methylene-amino) propyl) phthalamide. Journal of the Korean Chemical Society. 2011;55(3):418-29.
49.Shakdofa MM, Al-Hakimi AN, Elsaied FA, Alasbahi SO, Alkwlini A. Synthesis, characterization and bioactivity¬¬¬¬ Zn2+, Cu2+, Ni2+, Co2+, Mn2+, Fe3+, Ru3+, VO2+ and UO22+ complexes of 2-hydroxy-5-((4-nitrophenyl) diazenyl) benzylidene)-2-(p-tolyl-amino) acetohydrazide. Bulletin of the Chemical Society of Ethiopia. 2017;31(1):75-91.
50.Čobeljić B, Turel I, Pevec A, Jagličić Z, Radanović D, Anđelković K, et al. Synthesis, structures and magnetic properties of octahedral Co (III) complexes of heteroaromatic hydrazones with tetraisothiocyanato Co (II) anions. Polyhedron. 2018;155:425-32.
51.Salcedo-Abraira P, Vilela SM, Babaryk AA, Cabrero-Antonino M, Gregorio P, Salles F, et al. Nickel phosphonate MOF as efficient water splitting photocatalyst. Nano Research. 2021;14(2):450-7.
52.Saleh HA, Rahman ASAA, Al-Jeboori MJ. SYNTHESIS, STRUCTURAL CHARACTERISATION AND BIOLOGICAL EVALUATION OF NEW SEMICARBAZONE METAL COMPLEXES DERIVED FROM MANNICH-BASE. 2021;21(0976-1772):150-68.
53.El- Afify ME, Elsayed SA, Shalaby TI, Toson EA, El- Hendawy AM. Synthesis, characterization, DNA binding/cleavage, cytotoxic, apoptotic, and antibacterial activities of V (IV), Mo (VI), and Ru (II) complexes containing a bioactive ONS- donor chelating agent. Applied Organometallic Chemistry. 2021;35(2):e6082.